Taylor & Francis
Taylor & Francis Group

Isolation and Characterization of Cellulose Nanofibrils from Banana Pseudostem, Oil Palm Trunk, and Kenaf Bast Fibers Using Chemicals and High-intensity Ultrasonication

Mohammad Khairul Azhar Abdul Razab, Ros Syazmini Mohd Ghani, Farah Amanina Mohd Zin, Nik Alnur Auli Nik Yusoff & An'Amt Mohamed Noor

Taylor & Francis
Taylor & Francis Group

Check for updates

Isolation and Characterization of Cellulose Nanofibrils from Banana Pseudostem, Oil Palm Trunk, and Kenaf Bast Fibers Using Chemicals and High-intensity Ultrasonication

Mohammad Khairul Azhar Abdul Razab [a], Ros Syazmini Mohd Ghani[b], Farah Amanina Mohd Zin[c], Nik Alnur Auli Nik Yusoff[c], and An'Amt Mohamed Noor [c]

[a]School of Health Sciences, Universiti Sains Malaysia, Health Campus, Kubang Kerian, Kelantan, Malaysia; [b]School of Engineering and Technology, University College of Technology Sarawak, Sibu, Sarawak, Malaysia; [c]Bioengineering and Technology, Universiti Malaysia Kelantan, Jeli Campus, Jeli, Kelantan, Malaysia

ABSTRACT

The adoption of high-intensity ultrasonication in the isolation process of cellulose nanofibrils (CNF) as an economical, timesaving, and environmental-friendly process has been explored. Three types of raw organic fibers, i.e., banana pseudostem, oil palm trunk, and kenaf bast were analyzed for the production of CNF using the process mentioned earlier. Before the raw organic fibers were subjected to a high-intensity ultrasonication process, it underwent an alkaline treatment to eliminate the non-cellulosic compounds. Field emission scanning electron microscope (FESEM) and transmission electron microscope (TEM) micrographs confirmed the presence of nanofibrils in all three different types of CNF. The frequency, amplitude, and duration of ultrasonication used in this study were sufficient to produce CNF. Fourier-transform infrared spectroscopy (FTIR) results indicated that the chemical treatment employed in this paper was effective in removing the compounds, especially lignin and hemicellulose. The increase in crystallinity, which is one of the advantages of CNF, was observed from the X-ray diffraction (XRD) results. Hence, it can be deduced that high-intensity ultrasonication could simplify the complex process of CNF isolation compared to the conventional method, widening the utilization and source of CNF in the industry.

摘要

本研究提出了一种新颖的概念, 作为一种结构多样的反扭法, 生产出具有低余扭矩的超软特性纱线. 几何分析表明, 反向扭转应力的定期干预重塑了纱线结构中的纤维排列, 导致纤维运动轨迹从原来的同心螺旋到变形的非同心螺旋, 出现反向纤维段. 机械性能预测显示, 纱线表观结构倾斜角较低的反扭曲纱线的湿咆哮比具有相同扭曲力的较不扭曲纱线小得多. 然后, 对两次扭法产生的反扭曲纱线和扭纺率较低的纱线进行系统比较, 结果表明, 反扭纱线的残余扭矩和纱线强度比较少扭纱线低. 然而, 反扭曲的纱线有蓬松的结构与更多的毛性.

Introduction

Cellulose can be synthesized from plants, marine animals, fungi, as well as bacteria (Jiang and Hsieh 2013). It is the most abundant natural renewable and biodegradable polymer, with approximately 10^{12} tons of cellulose are synthesized and destroyed annually (Abraham *et al.*, 2011). Cellulose is a major

component of plant fiber that is primarily present in the secondary cell wall and plays a major role in providing strength (Sorieul et al. 2016; Sundqvist and Moren 2002).

Meanwhile, nanocellulose is a polysaccharide nanoparticle that can be obtained from cellulose (Mohd et al. 2016). Nanocellulose possesses several advantages, including large surface area, high aspect ratio, high Young's modulus, low cost, lightweight, relative abundance, renewable, and biodegradable (Li et al. 2015). Nanocellulose material has been used in numerous applications depending on its characteristics (Li et al. 2015). It can be designed to match other materials or as a reinforcing agent to increase the mechanical strength of a composite structure due to its high stiffness and strength (Lisdayana et al. 2020; Patchiya et al. 2018), easily modified to act as a water-filtration membrane for water treatment, as a stabilizer and thickening agent in numerous applications, e.g., paint (Linglong et al. 2019), food (Shuji, Eiji, and Katsushi 2017), adhesives and coatings (Martin et al. 2017; Raha et al. 2020), cement (Priyadarshana et al. 2020; Mocktar, Razab, and Noor 2020; Razab et al. 2019), and acts as a drug carrier (Salman, Amir, and Theo 2014; Shuji, Eiji, and Katsushi 2017) in human bodies and can be used as a wound dressing due to its size and antibacterial properties (Tibolla et al. 2014). Meanwhile, the high surface area-to-volume ratio of the nanocellulose offers high sensitivity and faster response as sensors compared to microcellulose (Mohaiyiddin et al. 2016).

Nanocellulose can be divided into two types, i.e., cellulose nanofibrils (CNF) and cellulose nanocrystal (CNC), based on their nanostructures. CNF is longer than the rod-like CNC (Jiang and Hsieh 2013). CNF is produced by the process of delamination of the hierarchical structure of the cellulosic fibers present in the plant cell wall (Velásquez-Cock et al. 2016). Furthermore, CNF possesses a stronger reinforcement capability than CNC in a polymer matrix because CNF has a much larger aspect ratio and stronger percolation network (Li et al. 2015). The specific characteristics of CNF are optical transparency, low thermal expansion coefficient, and high tensile strength (Velásquez-Cock et al. 2016).

The isolation process of cellulose nanoparticles usually involves two steps, i.e., a combination of enzymatic and chemical pretreatments with mechanical treatments despite the various methods of production (Desmaisons et al. 2017). Among the mechanical treatments that can be employed include crycocrushing (Alemdar and Sain 2008; Ayan, Mohini, and Mark 2005), grinding (Patchiya et al. 2018), refining, and high-pressure homogenization (Iwamoto et al. 2005; Kawee, Lam, and Sukyai 2018), high-pressure microfludisation (Fillat et al. 2018; Wei et al. 2012) and high-intensity ultrasonication (Abe, Iwamoto, and Yano 2007; Feng et al. 2018; Mocktar, Razab, and Noor 2020; Mohammad et al. 2014).

However, the current mechanical methods used in the extraction of large-scale CNF are restricted due to the high energy consumption of the fibrillation process (Desmaisons et al. 2017; Malucelli et al. 2018). Although the usage of high volume strong chemicals consumption during the chemical pulping process will give better results and uniform CNF size, it will cause a prolonged and non-environmentally friendly reaction process (Hongxiang, 2018). Thus, a new pilot set-up and the development of a low-cost, large-scale technique that allows minimal chemical hazards and improves the feasibility of high-quality CNF for future prospects (Mishra, Sabu, and Tiwari 2018), especially for the abundant local plant fibers, should be established in an environmentally friendly manner.

Herein, we combined minimal chemical treatments with a disintegration technique to reduce the pollution and energy consumption during the CNF isolation processes. We developed a novel technique to obtain CNF from a selection of local organic fibers, i.e., banana pseudostems, oil palm trunk, and kenaf bast using an alkaline treatment chemical pulping, followed by a high-intensity ultrasonication technique for mechanical disintegration. To the best of our knowledge, this technique is ideal for large-scale productions, requires minimal cost, rapid and only needs a simple two-steps method for a high purity CNF to be obtained.

Experimental

Materials

A bundle of banana pseudostem was obtained from Malaysian Agricultural Research and Development Institute (MARDI), while kenaf bast were obtained from the National Kenaf and Tobacco Board (LKTN), Kota Bharu, Malaysia and oil palm trunk was obtained from the Malaysian Palm Oil Board (MPOB), Selangor. These samples were used for the preparation of CNFs. Treatment and isolation of cellulose were done by using sodium hydroxide, sodium sulfite, and hydrogen peroxide, 30% received from Merck, Darmstadt, Germany.

Preparation, treatment, and isolation of cellulose nanofibrils (CNF)

The samples were shredded into micro size raw fibers before isolated by the pretreatment and bleaching processes. This is followed by mechanical disintegration. Before the pretreatment process, the fibers were initially cut into a smaller length of about 0.5 to 1 cm and oven-dried at 60°C for 24 h to eliminate any remaining moisture. The fibers were then immersed in 2.5 mol L^{-1} of NaOH and 0.4 mol L^{-1} of Na_2SO_3 to remove the lignin and hemicellulose as proposed by Wyman et al. (2005). The fibers were boiled for 8 h to speed up the process and rinsed in hot distilled water to eliminate any impurities. For this purpose, 2.5 mol L^{-1} of H_2O_2 was used as a bleaching agent, aided by heat, until the yellowish color had completely disappeared, which usually took about 6 h. The fibers were then rinsed with cold distilled water to remove more lignin content and the active hydroxyl group of cellulose (Salehudin et al. 2012). The treated fibers were filtered to get the cellulose prior to the air-drying process. Ultrasonic sonicator (Model: Q500, QSonica Sonicators) was used to sonicate the mixture of 0.4 g air-dried cellulose with 50 mL distilled water for 30 minutes to obtain the nanocellulose. The frequency was set at 20 kHz with 60% amplitude for 5 seconds on and 5 seconds off pulse. The summary of the overall process is shown in Figure 1.
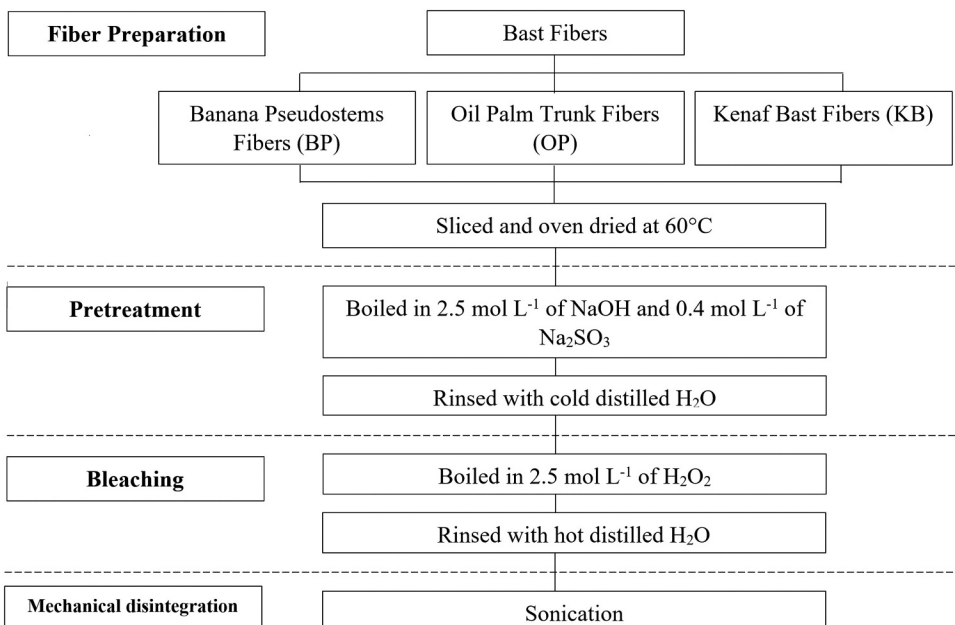

Figure 1. Preparation, treatment and isolation processes scheme of cellulose nanofibrils.

Characterization

Morphological analysis

The morphology of isolated CNF was studied using both the transmission electron microscope (TEM) and field emission scanning electron microscope (FESEM). For the TEM sample analysis preparation, a drop of CNF suspension was deposited on a copper grid and allowed to dry at room temperature. The images were obtained using JEOL JEM-2200FS equipped with an electron gun, at an accelerating voltage of 200 kV. While for the FESEM, a few drops of CNF suspension were placed on indium-tin oxide (ITO) coated glass and left to dry at room temperature. After drying, the samples were examined using Joel JSM-7900 F. The size of each fiber obtained from TEM and FESEM were randomly measured using the built-in scaling software for polydispersity analysis. The micrographs were then analyzed using the ImageJ software to determine the average distribution of the fiber size variation frequencies on a selected area, as shown by the arrows in Figures 2(a),3(a) and 4(a) for TEM images, and the regions of interest (ROI) in Figures 5(a),6(a) and 7(a) for FESEM micrograph. Diversity for each plant nanofibres was selected between the diameter of 20–50 nm ± 10 nm of the micrographs obtained, as shown in Figures 5(b),6(b), and 7(b).

FTIR spectroscopy

FTIR spectroscopy scanned the presences of any changes in the functional groups of raw organic fibers and freeze-dried CNF samples. The samples were dried at 60°C for 12 h before analysis. The spectra were viewed using the Thermo Scientific Nicolet iN10 Infrared Microscope and iZ10 FTIR Spectrometer machine. The transmittance mode was used with the spectra within the range of 4000–500 cm^{-1}, resolution 4 cm^{-1}, and average 100 scans.

X-ray diffraction

X-ray equatorial diffraction profiles of the fibers were collected using the Bruker D2 X-ray Diffractometer through CuKα radiation at the operating voltage and current of 30 kV and 20 mA. The diffraction intensities were recorded between 10° and 90° with the scanning range of 2θ. The crystallinity index (CrI) of the samples was calculated using Equation (1), following the method proposed by Segal et al. (1959). In this method, CrI was calculated as the ratio of heights between the maximum intensity of the crystalline peak close to 2θ = 22° (I_{200}) and the intensity of the non-crystalline material diffraction peak close to 2θ = 18° (I_{non-cr}).

Crystallinity index, CrI (%) = $(I_{crystalline} - I_{amorphous})/I_{crystalline} \times 100$ 　　　　　Eq. (1)
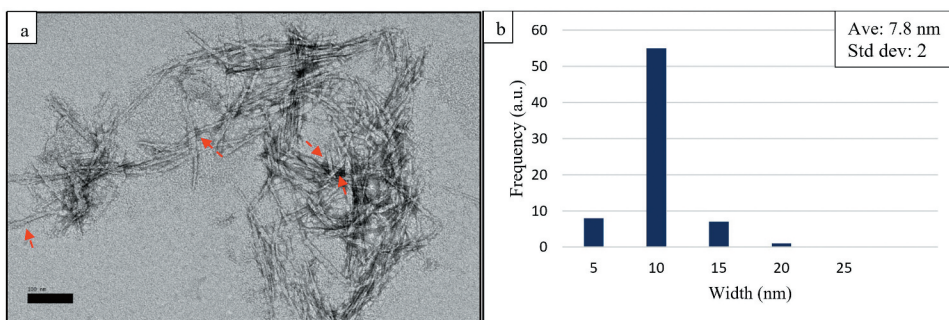

Figure 2. TEM images of CNF and its width distribution profile isolated from BPCNF; The red arrows point to CNF (a) with their average width (b) .

Results and discussion

TEM analysis

The presence of CNF obtained from the banana pseudostems (BPCNF), oil palm trunk (OPCNF), and kenaf bast (KBCNF) were confirmed by the TEM (Figures 2(a),3(a) and 4(a)). The average diameter of the BPCNF, OPCNF, and KBCNF is 7.8 nm, 11 nm, and 6.2 nm, as shown in Figures 2(b), 3(b) and 4 (b), respectively. The long, needlelike, and entangled cellulosic filaments structures of CNF obtained formed the network that corresponds to the definition of CNF as defined by Tibolla et al. (2017). This proves that high-intensity ultrasonication promotes cell wall defibrillation by breaking the bonds between the semi-crystalline fibers and releasing the CNF.

However, cellulose nanocrystals (CNC) are also present along the OPCNF, as shown in Figure 3(a). Application of the duration of sonification gives different results depending on the different types of fibers (Wenshuai et al. 2011). In this case, sonication duration might be a factor that causes the CNF being transformed to CNC for oil palm fibers. Meanwhile, dark spots were detected in all TEM images, indicating that the CNF were stacked onto each other due to agglomeration, as claimed by Mohaiyiddin et al. (2016). However, the spots observed could also be due to the deposition errors during sample grid preparation for TEM analysis. Figure 4(a) illustrates the agglomeration of KBCNF, which relates to the small size of CNF that creates a higher aspect ratio, which is the length to diameter ratio. The high aspect ratio creates an additional formation of interfibrillar hydrogen bonds between CNF that leads to greater agglomeration. Besides, Mohd et al. (2016) explained that agglomerates occur due to the hydrogen bond interactions between the hydroxyl groups on the CNF samples even after the sonication process.

Figure 3. TEM images of CNF and its width distribution profile isolated from OPCNF; The red arrows point to CNF (a) with their average width (b). The red circle shows the present of CNF and CNC.
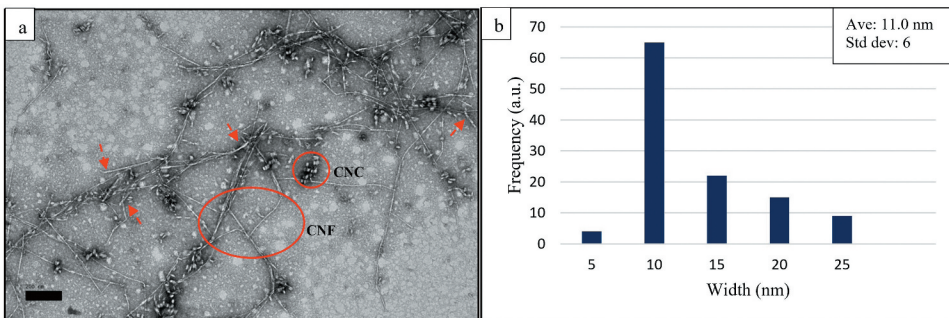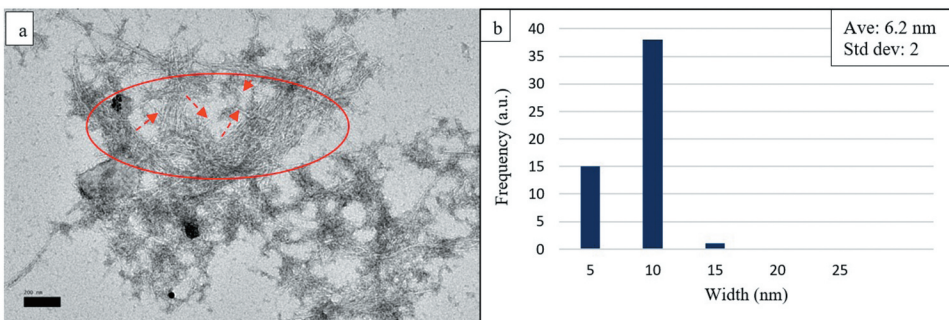

Figure 4. TEM images of CNF and its width distribution profile isolated from KBCNF. The red arrows point to CNF (a) with their average width (b) .

Figures 2(b), 3(b) and 4(b) indicate the width distribution profiles of BPCNF, OPCNF, and KBCNF, respectively. The width distributions show that all types of CNFs have an average width of 10 nm. The smallest nanofibrils have a diameter of approximately 5 nm. Among the three types of CNFs, BPCNF is the most polydisperse nanofibril, with a width distribution between 5 and 25 nm compared to the other CNFs.

FESEM analysis

The FESEM micrographs also confirm the presence of BPCNF, OPCNF, and KBCNF on the surface structures, as shown in Figures 5(a,b).6(a,b), and 7(a,b) FESEM images allow the observation of the entangled network of CNFs. However, the size distribution of the fibers differs from that of the TEM images for all fibers, where high polydispersity is observed on the sample surface, with varying measurements noted for some single fibrils. Meanwhile, the existence of some nanofibril networks within the sample structures gave high chances for improved accuracy measurement using TEM due to lower CNF polydispersity. The polydispersity of BPCNF, OPCNF, and KBCNF was analyzed using the broad width distribution profiles obtained from ImageJ software, as illustrated in Figures 5(b,c)6(b, c) and 7(b,c).
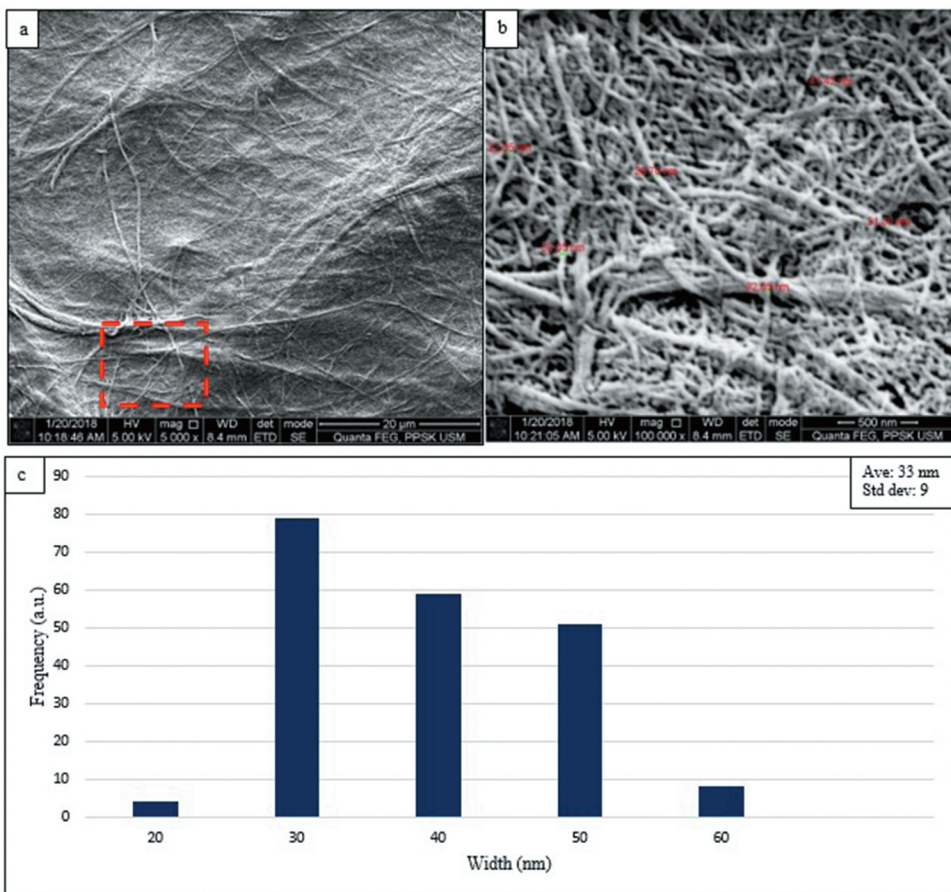

Figure 5. FESEM images of BPCNF with its focus area (red box) (a), zoomed image of focus area (b) random measurements of the fiber diameter and (c) the average width sizes of BPCNF distribution.

Figure 5(c) illustrates that the average width of BPCNF is between 30 and 50 nm in diameter, in line with the findings of Velásquez-Cock et al. (2016) and Zuluaga et al. (2009). Moreover, Khawas and Deka (2016) who studied the CNF from banana pseudostems using high-intensity ultrasonication concluded that the width distribution is between 20 and 35 nm, where the CNF diameter will decrease when the output power of ultrasonication is increased.

Meanwhile, the width of OPCNF obtained is smaller than BPCNF, where the average width is between 20 and 30 nm, as shown in Figure 6(c). Furthermore, the width of CNF is contradicted with some previous research findings, where the average size of CNF obtained from oil palm frond was 44.7 nm (Mohaiyiddin et al. 2016) and 4 to 15 nm for CNF from the Oil Palm Empty Fruit Bunch (OPEFB; Lani et al. 2014). This shows that different parts of the oil palm will produce different size of CNFs, depending on its physical and mechanical structures. The average width distribution of KBCNF is almost similar to BPCNF, i.e., between 30 and 40 nm (Figures 7(c)). The KBCNF sizes obtained using this method are also in line with the grinding method studied by Karimi et al. (2014).
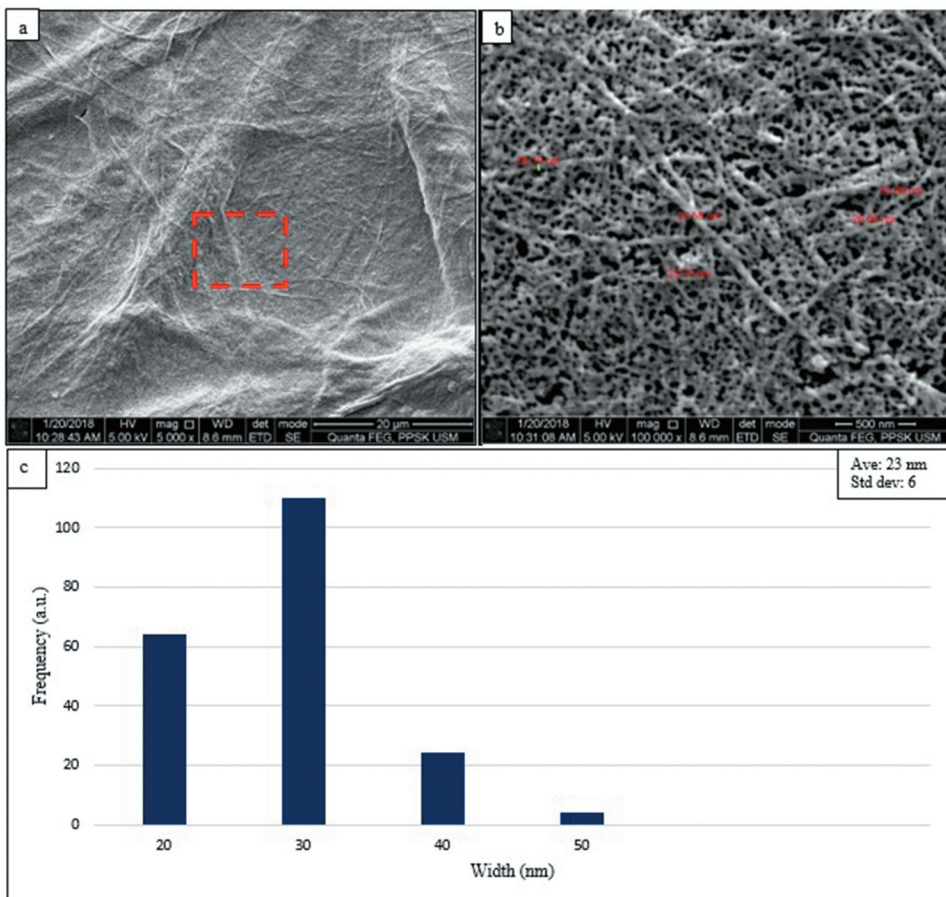

Figure 6. FESEM images of OPCNF with its focus area (red box) (a), zoomed image of focus area (b) random measurements of the fiber diameter and (c) the average width sizes of OPCNF distribution.
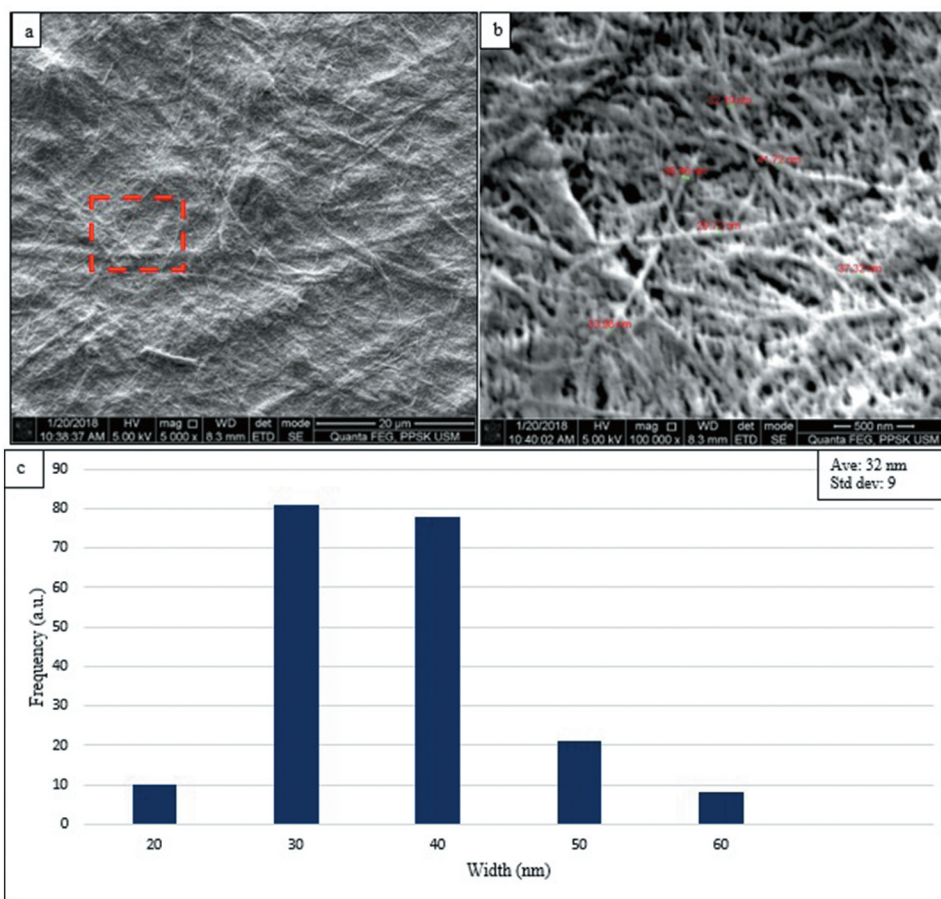
Figure 7. FESEM images of KBCNF with its focus area (red box) (a), zoomed image of focus area (b) random measurements of the fiber diameter and (c) the average width sizes of KBCNF distribution.

FTIR analysis

Figure 8 reveals the FTIR spectra of raw organic fibers and the CNF for banana pseudostem, oil palm trunk, and kenaf bast. The main components of the plant, which include cellulose, hemicellulose, and lignin, are typically composed of alkenes, esters, aromatics, ketones, and alcohol Morán et al. 2008.

The FTIR spectra of all samples exhibit a broadband in the region of 3500–3200 cm^{-1} indicating a free OH stretching vibration in the cellulose molecules (Figure 8[i]). It is the primary functional group of cellulose and has been discussed by fellow researchers (Deepa et al. 2015; Espinosa et al. 2017; Mandal and Chakrabarty 2011). Similarly, the CH group, mainly composed of alkyl and aliphatic compounds in cellulose, is detected at 2900 cm^{-1}, as illustrated in Figure 8(ii). An additional peak at the range of 1600 cm^{-1} that denotes OH is present in both raw organic fibers and their CNFs (Figure 8 [iv]). This peak is related to the water absorbed by the cellulose (Karimi et al. 2014; Sulaiman et al. 2015; Velásquez-Cock et al. 2016). The appearance of this peak in the spectra is probably due to the reaction of sodium hydroxide (NaOH) with the OH groups from the cellulose and the subsequent formation of water molecules. Even though the CNF was subjected to the drying process, the water adsorbed in the cellulose molecules was not eliminated due to the natural cellulose–water interactions (Lani et al. 2014). Conclusively, the original molecular structure of the cellulose is almost maintained even for the CNF samples.
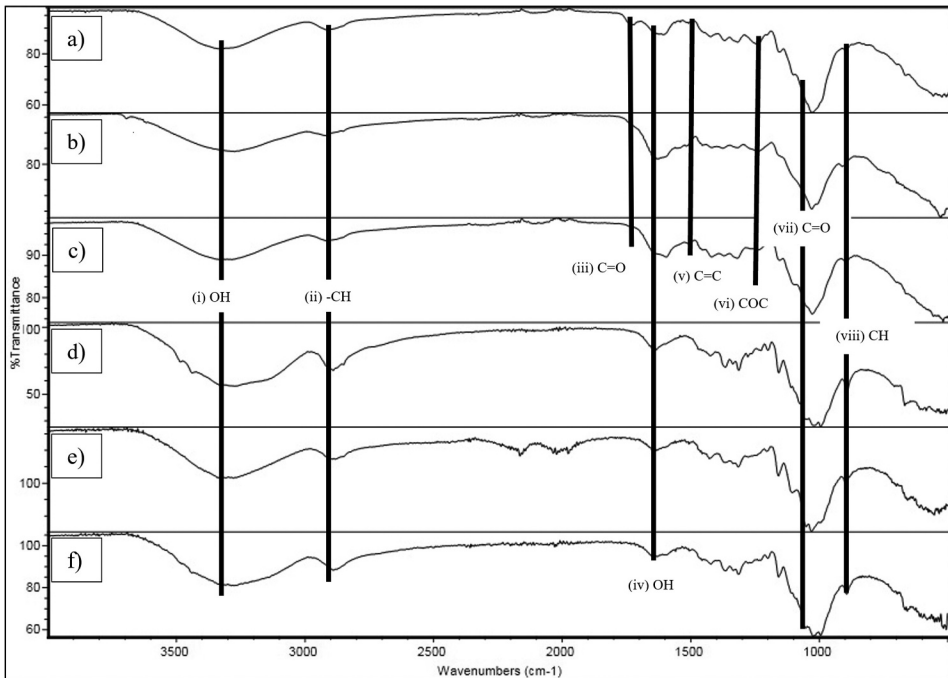
Figure 8. FTIR spectra in 4000–500 cm^{-1} range for a) BP, b) OPT, c) KB, d) BCNF, e) OPCNF, f) KCNF.

Throughout the isolation process of the CNF from the raw organic fibers, a few changes had occurred in the functional groups of the samples. In general, as observed from Figure 8, the intensity of the peak for CNF samples inclines after the chemical and sonication treatment due to an increase in the concentration of OH as the alkaline reduces the hydrogen bonding in the cellulosic hydroxyl groups resulting in the absence of a peak associated with hemicellulose and lignin. The peak is present only in the spectrum of approximately 1700 cm^{-1} (Figure 8[iii]), which corresponds to C = O stretching in the acetyl and uronic ester groups of hemicellulose or the ester carbonyl groups in the *p*-coumaric units of lignin. The presence of this peak was also reported by other researchers (Joonobi et al. 2010; Karimi et al. 2014; Kim et al. 2016; Lani et al. 2014). On a similar note, Chieng et al. (2017) reported that the disappearance of the peak after an alkaline treatment was due to the removal of the carboxylic groups, which may contain traces of fatty acids on the surface of the fiber.

The peak between 1500 and 1600 cm^{-1} (Figure 8[v]) describes C = C in the aromatic ring vibration of the lignin. The absence of these peaks in the CNF samples proved the absence of lignin after the isolation process of the CNF. The absence of the peak was also discussed by Reddy and Yang (2005), Morán et al. (2008), and Ludueña et al. (2011). The peak, in the range of 1200 cm^{-1} (Figure 8[vi]), can be observed in three different types of fibers, i.e., 1241 cm^{-1} for banana pseudostem (BP), 1238 cm^{-1} for oil palm trunk (OPT), and 1231 cm^{-1} for kenaf bast (KB). The vibration peak is related to the C-O-C stretching of the aryl-alkyl ether. The disappearance of the peaks in all CNF samples was due to the alkaline treatment using NaOH that removed most of the lignin from the samples (Joonobi et al. 2010; Lani et al. 2014; Sulaiman et al. 2015). The peak is seen at 1029 cm^{-1} for the banana fiber, 1027 cm^{-1} for the kenaf fiber, and 1035 cm^{-1} for the oil palm fiber, and they are characterized as the C = O band structure of alcohol functional group (Figure 8[viii]). The disappearance of the peak after alkaline treatment in this study was also reported by Bakri and Jayamani (2016).

Overall, the CNF obtained in this study is considered pure, i.e., it contains a very small amount of lignin and other non-cellulosic substances. It validates the removal of hemicellulose through alkaline

treatment because the alkali cleaved the esoteric bond easily. In addition, xylose in the hemicellulose was converted into a water-soluble material and wiped out during the water-rinsing process.

XRD analysis

The quantitative study on cellulose crystallinity was carried out to understand the effect of treatment on raw organic fiber to produce CNF. The peak intensities and peak position of the X-ray diffractogram for three types of raw organic fibers and their CNF is depicted in Figure 9.
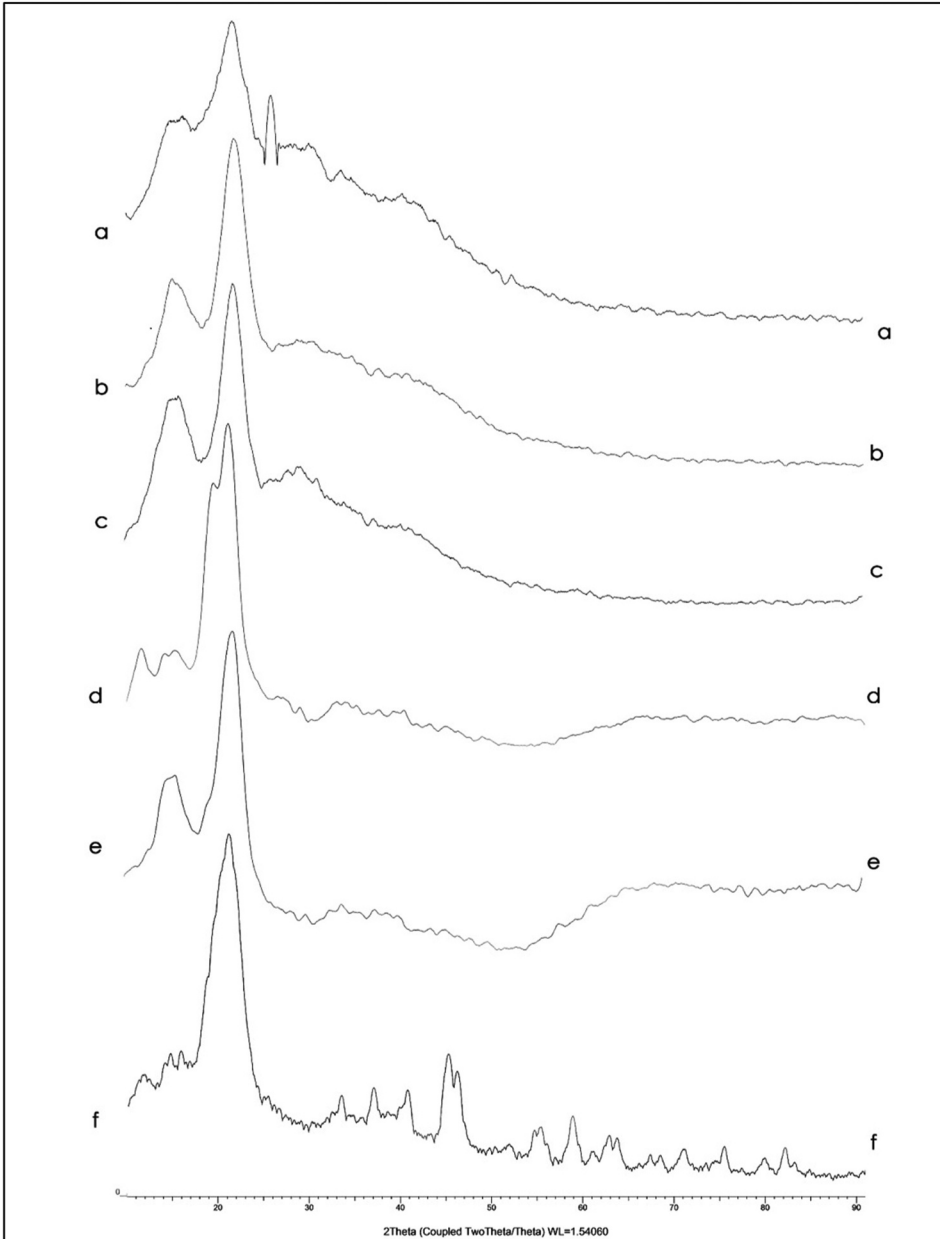

Figure 9. XRD diffraction profiles in 10–90° range for a) BP, b) OPT, c) KB, d) BCNF, e) OPCNF, f) KCNF.

Table 1. The crystallinity index of fiber and its CNF.

	Banana Pseudostem		Oil Palm Trunk		Kenaf Bast	
	Raw	CNF	Raw	CNF	Raw	CNF
CrI (%)	29.1	50.7	17.6	36.4	29.6	59.1
Change (%)	74.23		106.82		99.66	

All diffractograms displayed the typical peaks of semi-crystalline materials that consist of a broad hump amorphous region and the sharp, intense peak of the crystalline region. The peaks occurred at approximately $2\theta = 22.36°$, $27.47°$, and $22.36°$ for BP, OPT, and KB fibers. The peaks are related to the typical type of cellulose I, which is the natural type of plant cellulose with two polymorphs, I_α and I_β (Janardhnan and Sain 2011; Kim et al. 2016; Nobuta et al. 2016). Whereas the peak of CNF is sharper and more intense compared to the raw fibers, indicating that the sample is more crystalline. At the CNF diffractogram, the peaks are at $2\theta = 21.95°$, $22.77°$, and $22.79°$ for BPCNF, OPCNF, and KBCNF, respectively. Usually, during the NaOH treatment, cellulose I structure will be destroyed by the separation of molecular chains and reformed into cellulose II. However, in this study, cellulose II was not detected. Similar findings have been discussed by Fahma et al. (2010), Mohaiyiddin et al. (2016), and Rambabu et al. (2016).

The peak in the diffractogram is also used to relate to the crystallinity of the material, i.e., CrI (Yusuf et al. 2019). The crystallinity index of the fiber and its CNF is shown in Table 1. The crystallinity of the CNF is higher than its raw fibers for all three plant samples. The CNF crystallinity changed to 74.23% for BNCNF, 106.82% for OPCNF, and 99.6% for KBCNF from their raw fibers (Table 1). The results further revealed that the high-intensity ultrasonication used in this study disrupted the weak amorphous regions of the cellulose fibers, which led to the molecular separation process to obtain more individual cellulose fibers. In addition, the ultrasonication duration is sufficient and does not lead to the destruction of cellulose crystallinity. The increase in the crystallinity is due to the partial elimination of hemicellulose and lignin from the fiber during the alkali treatment (Mocktar, Razab, and Noor 2020), as discussed in the FTIR results. The treatment process might reduce the amorphous regions, where most of the molecule structures consist of nanocellulose. Mussatto et al. (2008) stated that the removal of the hemicelluloses and lignin extensively altered the structure of the natural fibers, increasing the crystal surface area, and the accessibility of the hydrolytic agent to the cellulose. These findings support the claim that the chemical treatment can efficiently remove the non-cellulosic amorphous polysaccharides.

Conclusion

The present work revealed that the banana pseudostem, oil palm trunk, and kenaf bast fibers could be used as raw materials for the production of high-quality CNF using a combination of chemical treatments, followed by sonication process. Chemically purified cellulose was isolated using high-intensity ultrasonication that would help in the homogenization, tailoring, and size reduction of CNF. TEM images confirmed the presence of nanofibrils and the width distribution profiles drawn from FESEM helped to understand the polydispersed diameter of nanofibrils. The FTIR spectra exemplified that the treatment employed in this study substantially removed the hemicellulose and lignin. The XRD diffractograms exhibited sharp peaks at 2θ, which demonstrated type I cellulose. Thereby, this study favorably justified the production of CNF from three different bast fibers, i.e., banana pseudostems, oil palm trunk, and kenaf bast. It opens up more possibilities in the manufacturing of CNF from various types of natural fibers, with numerous applications.

ORCID

Mohammad Khairul Azhar Abdul Razab 🆔 http://orcid.org/0000-0001-5788-8176
An'Amt Mohamed Noor 🆔 http://orcid.org/0000-0003-1918-5765

References

Abe, K., S. Iwamoto, and H. Yano. 2007. Obtaining cellulose nanofibers with a uniform width of 15 nm from wood. *Biomacromolecules* 8:3276–78. doi:10.1021/bm700624p.

Abraham, E., B. Deepa, L. A. Pothan, M. Jacob, S. Thomas, U. Cvelbar, and R. Anandjiwala. 2011. Extraction of nanocellulose fibrils from lignocellulosic fibres: A novel approach. *Carbohydrate Polymers* 86:1468–75. doi:10.1016/j.carbpol.2011.06.034.

Alemdar, A., Sain, M., 2008. Isolation and characterization of nanofibers from agri-cultural residues: wheat straw and soy hulls. Bioresour. Technol. 99, 1664–1671

Ayan, C., S. Mohini, and K. Mark. 2005. Cellulose microfibrils: A novel method of preparation using high shear refining and cryocrushing. *Holzforschung* 59:102–07. doi:10.1515/HF.2005.016.

Bakri, M. K. B., and E. Jayamani. 2016. Comparative study of functional groups in natural fibers: Fourier transform infrared analysis (FTIR). *Futuristic Trends in Engineering, Science, Humanities, and Technology* 16:167–74.

Chandra, J., N. George, and S. K. Narayanankutty. 2016. Isolation and characterization of cellulose nanofibrils from areca nut husk fibre. *Carbohydrate Polymers* 142:158–66. doi:10.1016/j.carbpol.2016.01.015.

Chieng, B. W., S. H. Lee, N. A. Ibrahim, Y. Y. Then, and Y. Y. Loo. 2017. Isolation and characterization of cellulose nanocrystals from oil palm mesocarp fiber. *Polymers* 9:1–11. doi:10.3390/polym9080355.

Deepa, B., E. Abraham, N. Cordeiro, M. Mozetic, A. P. Mathew, K. Oksman, M. Faria, S. Thomas, and L. A. Pothan. 2015. Utilization of various lignocellulosic biomass for the production of nanocellulose: A comparative study. *Cellulose* 22:1075–90. doi:10.1007/s10570-015-0554-x.

Desmaisons, J., E. Boutonnet, M. Rueff, A. Dufresne, and J. Bras. 2017. A new quality index for benchmarking of different cellulose nanofibrils. *Carbohydrate Polymers* 174:318–29. doi:10.1016/j.carbpol.2017.06.032.

Espinosa, E., R. Sánchez, Z. González, J. Domínguez-Robles, B. Ferrari, and A. Rodríguez. 2017. Rapidly growing vegetables as new sources for lignocellulose nanofibre isolation: Physicochemical, thermal and rheological characterization. *Carbohydrate Polymers* 175:27–37. doi:10.1016/j.carbpol.2017.07.055.

Fahma, F., Iwamoto, S., Hori, N., Iwata, T. and Takemura, A. (2010). Isolation, preparation, and characterization of nanofibers from oil palm empty-fruit-bunch (OPEFB), Cellulose, 17:977–985

Feng, Y. H., T. Y. Cheng, W. G. Yang, P. T. Ma, H. Z. He, X. C. Yin, and X. X. Yu. 2018. Characteristics and environmentally friendly extraction of cellulose nanofibrils from sugarcane bagasse. *Industrial Crops and Products* 111:285–91. doi:10.1016/j.indcrop.2017.10.041.

Fillat, Ú., B. Wicklein, R. Martín-Sampedro, D. Ibarra, E. Ruiz-Hitzky, C. Valencia, A. Sarrión, E. Castro, and M. E. Eugenio. 2018. Assessing cellulose nanofiber production from olive tree pruning residue. *Carbohydrate Polymers* 179:252–61. doi:10.1016/j.carbpol.2017.09.072.

Hongxiang, X., D. Haishun, Y. Xianghao, and S. Chuanling. 2018. Recent strategies in preparation of cellulose nanocrystals and cellulose nanofibrils derived from raw cellulose materials. *International Journal of Polymer Science* 2018:1–25.

Iwamoto, S., A. N. Nakagaito, H. Yano, and M. Nogi. 2005. Optically transparent composites reinforced with plant fibre-based nanofibers. *Applied Physics A* 81:1109–12. doi:10.1007/s00339-005-3316-z.

Janardhnan, S., and M. M. Sain. 2011. Targeted disruption of hydroxyl chemistry and crystallinity in natural fibres for the isolation of cellulose nano-fibers via enzymatic treatment. *BioResources* 6:1242–50.

Jiang, F., and Y. L. Hsieh. 2013. Chemically and mechanically isolated nanocellulose and their self-assembled structures. *Carbohydrate Polymers* 95:32–40. doi:10.1016/j.carbpol.2013.02.022.

Jonoobi, M., R. Oladi, Y. Davoudpour, K. Oksman, A. Dufresne, Y. Hamzeh, and R. Davoodi. 2015. Different preparation methods and properties of nanostructured cellulose from various natural resources and residues: A review. *Cellulose* 22:935–69. doi:10.1007/s10570-015-0551-0.

Joonobi, M., J. Harun, P. M. Tahir, L. H. Zaini, S. SaifulAzry, and M. D. Makinejad. 2010. Characteristic of nanofibers extracted from kenaf core. *BioResources* 5:2556–66.

Kargarzadeh, H., M. Ioelovich, I. Ahmad, S. Thomas, and A. Dufresne. 2017. Methods for extraction of nanocellulose from various sources. In *In Handbook of nanocellulose and cellulose nanocomposites*, ed. H. Kargarzadeh, I. Ahmad, S. Thomas, and A. Dufresne., Vol. 1, 1–49. Weinheim: Wiley-VCH.

Kargarzadeh, H., I. Ahmad, I. Abdullah, A. Dufresne, S. Y. Zainudin, and R. M. Sheltami. 2012. Effects of hydrolysis conditions on the morphology, crystallinity, and thermal stability of cellulose nanocrystals extracted from kenaf bast fibers. *Cellulose* 19:855–66. doi:10.1007/s10570-012-9684-6.

Karimi, S., P. M. Tahir, A. Karimi, A. Dufresne, and A. Abdulkhani. 2014. Kenaf bast cellulosic fibers hierarchy: A comprehensive approach from micro to nano. *Carbohydrate Polymers* 101:878–85. doi:10.1016/j.carbpol.2013.09.106.

Kawee, N., N. T. Lam, and P. Sukyai. 2018. Homogenous isolation of individualized bacterial nanofibrillated cellulose by high pressure homogenization. *Carbohydrate Polymers* 179:394–401. doi:10.1016/j.carbpol.2017.09.101.

Khawas, P., and S. C. Deka. 2016. Isolation and characterization of cellulose nanofibers from culinary banana peel using high-intensity ultrasonication combined with chemical treatment. *Carbohydrate Polymers* 137:608–16. doi:10.1016/j.carbpol.2015.11.020.

Kim, D. Y., B. M. Lee, D. H. Koo, P. H. Kang, and J. P. Jeun. 2016. Preparation of nanocellulose from a kenaf core using E-beam irradiation and acid hydrolysis. *Cellulose* 23:3039–49. doi:10.1007/s10570-016-1037-4.

Lani, N. S., N. Ngadi, A. Johari, and M. Jusoh. 2014. Isolation, characterization, and application of nanocellulose from oil palm empty fruit bunch fiber as nanocomposites. *Journal of Nanomaterials* 2014:1–9. doi:10.1155/2014/702538.

Li, M. C., Q. Wu, K. Song, S. Lee, Y. Qing, and Y. Wu. 2015. Cellulose nanoparticles: Structure–morphology–rheology relationships. *ACS Sustainable Chemistry & Engineering* 3:821–32. doi:10.1021/acssuschemeng.5b00144.

Linglong, K., X. Dandan, H. Zaixin, W. Fengqiang, G. Shihan, F. Jilong, P. Xiya, D. Xiaohan, D. Xiaoying, L. Baoxuan, et al. 2019. Nanocellulose-reinforced polyurethane for waterbornewood coating. *Molecules* 24:1–13.

Lisdayana, N., F. Fahma, T. C. Sunarti, and E. S. Iriani. 2020. Thermoplastic starch–PVA nanocomposite films reinforced with nanocellulose from oil palm empty fruit bunches (OPEFBs): Effect of starch type. *Journal of Natural Fibers* 17:1069–80. doi:10.1080/15440478.2018.1558142.

Ludueña, L., D. Fasce, V. A. Alvarez, and P. M. Stefani. 2011. Nanocellulose from rice husk following alkaline treatment to remove silica. *BioResources* 6:1440–53.

Malucelli, L. C., M. M. Jordao, C. Lomonaco, D. Lacerda, L. G. Carvalho Filho, M. A. S. Carvalho Filho, and W. L. E. Magalhães. 2018. Influence of cellulose chemical pretreatment on energy consumption and viscosity of produced cellulose nanofibers (CNF) and mechanical properties of nanopaper. Cellulose 26::1667–81. doi:doi:10.1007/s10570-018-2161-0

Mocktar, F. A., Razab, M. K. A. A. and Noor, A. M. 2020. Incorporating kenaf and oil palm nanocellulose in building materials for indoor radon gas emanation reduction. *Radiation Protection Dosimetry* 189:69–75

Mocktar, N. A., Razab, M. K. A. A., Noor, A. M. and Abdullah, N. H. 2020. Preparation and characterization of kenaf and oil palm nanocellulose by acid hydrolysis method. Materials Science Forum 1010:495–500

Mohammad, T. I., M. A. Mohammad, P. Alessia, M. Alessio, and Z. Marina. 2014. Preparation of Nanocellulose: A Review. *AATCC Journal of Research* 1: 17–23.

Mohd, N. H., N. F. H. Ismail, J. I. Zahari, W. Fathilah, H. Kargarzadeh, S. Ramli, I. Ahmad, M. A. Yarmo, and R. Othaman. 2016. Effect of aminosilane modification on nanocrystalline cellulose properties. *Journal of Nanomaterials* 2016:1–8. doi:10.1155/2016/4804271.

Morán, J. I., V. A. Alvarez, V. P. Cyras, and A. Vázquez. 2008. Extraction of cellulose and preparation of nanocellulose from sisal fibers. *Cellulose* 15:149–59. doi:10.1007/s10570-007-9145-9.

Mussatto, S. I., M. Fernandes, A. M. Milagres, and I. C. Roberto. 2008. Effect of hemicellulose and lignin on enzymatic hydrolysis of cellulose from brewer's spent grain. *Enzyme and Microbial Technology* 43:124–29. doi:10.1016/j.enzmictec.2007.11.006.

Nobuta, K., H. Teramura, H. Ito, C. Hongo, H. Kawaguchi, C. Ogino, A. Kondo, and T. Nishino. 2016. Characterization of cellulose nanofiber sheets from different refining processes. *Cellulose* 23:403–14. doi:10.1007/s10570-015-0792-y.

Patchiya, P., R. Prasert, H. Xiaogang, X. Guangwen, A. Abuliti, and G. Guoqing. 2018. Nanocellulose: Extraction and application. *Carbon Resources Conversion* 1:32–43. doi:10.1016/j.crcon.2018.05.004.

Priyadarshana, R. W. I. B., P. E. Kaliyadasa, S. R. W. M. C. J. K. Ranawana, and K. G. C. Senarathna. 2020. Biowaste management: Banana fiber utilization for product development. *Journal of Natural Fibers* 17:1–11. doi:10.1080/15440478.2020.1776665.

Raha, S., B. Nikolay, M. L. Amine, S. Suraj, L. Igor, and M. Sergiy. 2020. Adhesion and stability of nanocellulose coatings on flat polymer films and textiles. *Molecules* 25:2–18.

Rambabu, N., S. Panthapulakkal, M. Sain, and A. K. Dalai. 2016. Production of nanocellulose fibers from pinecone biomass: Evaluation and optimization of chemical and mechanical treatment conditions on mechanical properties of nanocellulose films. *Industrial Crops and Products* 83:746–54. doi:10.1016/j.indcrop.2015.11.083.

Razab, M. K. A. A., R. S. M. Ghani, A. M. Noor, N. A. Mocktar, F. A. M. Zin, N. H. Abdullah, N. A. A. N. Yusuf, and M. Mohamed. 2019. Kenaf cellulose nanofibrils as mechanical enhancers of composite brick. *AIP Conference Proceedings* 2068:020071–1–020047–5.

Reddy, N., and Y. Yang. 2005. Structure and properties of high quality natural cellulose fibres from cornstalks. *Polymer* 46:5494–500. doi:10.1016/j.polymer.2005.04.073.

Salehudin, M. H., E. Saleh, I. Ida, S. Nur, and H. Mamat. 2012. Cellulose nanofibre isolation and its fabrication into bio-polymer - A review. Paper Presented at International Conference on Agricultural and Food Engineering for Life (Cafei2012), Putrajaya, Malaysia, November 26.

Salman, S., S. Amir, and G. M. V. D. V. Theo. 2014. Electroacoustic characterization of conventional and electrosterically stabilized nanocrystalline celluloses. *Journal of Colloid and Interface Science* 432:151–57. doi:10.1016/j.jcis.2014.06.061.

Segal, L. G. J. M. A., J. J. Creely, A. E. Martin, and C. M. Conrad. 1959. An empirical method for estimating the degree of crystallinity of native cellulose using the X-ray diffractometer. *Textile Research Journal* 29:786–94. doi:10.1177/004051755902901003.

Shuji, F., T. Eiji, and K. Katsushi. 2017. Nanocellulose-stabilized pickering emulsions and their applications. *Science and Technology of Advanced Materials* 18:959–71. doi:10.1080/14686996.2017.1401423.

Sorieul, M., A. Dickson, S. J. Hill, and H. Pearson. 2016. Plant fibre: Molecular structure and biomechanical properties, of a complex living material, influencing its deconstruction towards a biobased composite. *Materials* 9:1–36. doi:10.3390/ma9080618.

Sulaiman, H. S., C. H. Chan, C. H. Chia, S. Zakaria, and S. N. S. Jaafar. 2015. Isolation and fractionation of cellulose nanocrystals from kenaf core. *Sains Malaysiana* 44:1635–42.

Sulaiman, S., M. N. Mokhtar, M. N. Naim, A. S. Baharuddin, M. A. M. Salleh, and A. Sulaiman. 2016. Development of cellulose nanofibre (cnf) derived from kenaf bast fibre and it's potential in enzyme immobilization support. *Malaysian Journal of Analytical Sciences* 20:309–17. doi:10.17576/mjas-2016-2002-12.

Sundqvist, B., and T. Moren. 2002. The influence of wood polymers and extractives on wood colour induced by hydrothermal treatment. *European Journal of Wood and Wood Products* 60:375–76. doi:10.1007/s00107-002-0320-2.

Tibolla, H., F. M. Pelissari, M. I. Rodrigues, and F. C. Menegalli. 2017. Cellulose nanofibres produced from banana peel by enzymatic treatment: Study of process conditions. *Industrial Crops and Products* 95:664–74. doi:10.1016/j.indcrop.2016.11.035.

Tibolla, H., Pelissari, F. M. and Menegalli, F. C. (2014). Cellulose nanofibers produced from banana peel by chemical and enzymatic treatment, Food Science and Technology 59, 1311–1318

Velásquez-Cock, J., C. Castro, P. Gañán, M. Osorio, J. L. Putaux, A. Serpa, and R. Zuluaga. 2016. Influence of the maturation time on the physico-chemical properties of nanocellulose and associated constituents isolated from pseudostems of banana plant c.v. valery. *Industrial Crops and Products* 83:551–60. doi:10.1016/j.indcrop.2015.12.070.

Wei, L. J., X. Wang, Q. Chen, J. Chang, G. Kong, L. Su, and Y. Liu. 2012. Homogeneous isolation of nanocellulose from sugarcane bagasse by high pressure homogenization. *Carbohydrate Polymers* 90:1609–13. doi:10.1016/j.carbpol.2012.07.038.

Wenshuai, C., Y. Haipeng, L. Yixing, H. Yunfei, Z. Mingxin, and C. Peng. 2011. Isolation and characterization of cellulose nanofibres from four plant cellulose fibres using a chemical-ultrasonic process. *Cellulose* 18:433–42. doi:10.1007/s10570-011-9497-z.

Wyman, C. E., B. E. Dale, R. T. Elander, M. Holtzapple, M. R. Ladisch, and Y. Y. Lee. 2005. Comparative sugar recovery data from laboratory scale application of leading pretreatment technologies to corn stover. *Bioresources Technology* 96:2026–32. doi:10.1016/j.biortech.2005.01.018.

Yusuf, N. A. A. N., M. K. A. A. Razab, M. B. A. Bakar, K. J. Yen, C. W. Tung, R. S. M. Ghani, and M. N. Nordin. 2019. Determination of structural, physical, and thermal properties of biocomposite thin film from waste banana peel. *Jurnal Teknologi* 81:91–100.

Zuluaga, R., J. L. Putaux, J. Cruz, J. Vélez, M. I. Ganan, and P. Gañán. 2009. Cellulose microfibrils from banana rachis: Effect of alkaline treatments on structural and morphological features. *Carbohydrate Polymers* 76:51–59. doi:10.1016/j.carbpol.2008.09.024.